Aryl Hydrocarbon Receptor Activation in Pulmonary Alveolar Epithelial Cells Limits Inflammation and Preserves Lung Epithelial Cell Integrity

Elizabeth Zimmerman,* Anne Sturrock,*,† Christopher A. Reilly,‡ Katherine L. Burrell-Gerbers,‡ Kristi Warren,*,† Mustafa Mir-Kasimov,*,† Mingyang A. Zhang,* Megan S. Pierce,* My N. Helms,* and Robert Paine III*,†

The aryl hydrocarbon receptor (AHR) is a receptor/transcription factor widely expressed in the lung. The physiological roles of AHR expressed in the alveolar epithelium remain unclear. In this study, we tested the hypothesis that alveolar epithelial AHR activity plays an important role in modulating inflammatory responses and maintaining alveolar integrity during lung injury and repair. AHR is expressed in alveolar epithelial cells (AECs) and is active. AHR activation with the endogenous AHR ligand, FICZ (5,11-dihydroindolo[3,2-*b*] carbazole-6-carboxaldehyde), significantly suppressed inflammatory cytokine expression in response to inflammatory stimuli in primary murine AECs and in the MLE-15 epithelial cell line. In an LPS model of acute lung injury in mice, coadministration of FICZ with LPS suppressed protein leak, reduced neutrophil accumulation in BAL fluid, and suppressed inflammatory cytokine expression in lung tissue and BAL fluid. Relevant to healing following inflammatory injury, AHR activation suppressed TGF-β–induced expression of genes associated with epithelial–mesenchymal transition. Knockdown of AHR in primary AECs with shRNA or in CRISPR-Cas-9–induced MLE-15 cells resulted in upregulation of α-smooth muscle actin (*αSma*), *Col1a1*, and *Fn1* and reduced expression of epithelial genes *Col4a1* and *Sdc1*. MLE-15 clones lacking AHR demonstrated accelerated wound closure in a scratch model. AHR activation with FICZ enhanced barrier function (transepithelial electrical resistance) in primary murine AECs and limited decline of transepithelial electrical resistance following inflammatory injury. AHR activation in AECs preserves alveolar integrity by modulating inflammatory cytokine expression while enhancing barrier function and limiting stress-induced expression of mesenchymal genes. ***The Journal of Immunology*****, 2024, 213: 600–611.**

The aryl hydrocarbon receptor (AHR) is an intracellular receptor/transcription factor that is widely expressed in the lung (1). It is perhaps best known as a receptor for environmental toxicants, including a number that are components of air pollution. After binding these ligands, AHR moves to the nucleus and forms a heterodimer with the AHR nuclear translocator. It then binds to DNA sequences in the promoters of a large group of target genes to initiate transcription. However, in addition to its role in xenobiotic metabolism, interactions with a variety of endogenous AHR ligands contribute to regulation of cellular differentiation, proliferation, and survival in a number of tissues. Recent work suggests that AHR plays important roles in the pulmonary response to stress beyond its roles in normal homeostasis and xenobiotic metabolism (2–4).

The pulmonary alveolar epithelium is an enormous site of interaction with the outside world. Maintenance of alveolar epithelial barrier function is crucial for pulmonary gas exchange; disruption of this barrier in the setting of acute inflammation leads to lung injury and, in severe cases, to the acute respiratory distress syndrome (5). Beyond this barrier role, alveolar epithelial cells (AECs) play critical roles contributing to the innate immune milieu in the lung (6). They are the major source of GM-CSF in the lung, which drives functional maturation of alveolar macrophages (7). They also serve as sentinel cells, expressing early response cytokines (such as TNF-α and IL-1β) and chemokines (such as CXCL2) in response to local inflammatory stimulation (6, 8). A critical sequence in repair following injury involves type II AEC proliferation, migration, and differentiation to restore an intact, normally functioning epithelium (9). However, during this process, dysregulated epithelial–mesenchymal transition (EMT) (10) may lead to aberrant repair and pulmonary fibrosis. Because AHR activity can either worsen or ameliorate disease, depending on the cellular environment and specific ligand receptor activation (reviewed in (11)), the present studies were undertaken to test the hypothesis that endogenous ligand activation of AHR activity plays an important role in limiting proinflammatory signaling, thereby maintaining alveolar epithelial integrity, and limiting dysfunctional repair.

*Division of Respiratory, Critical Care and Occupational Pulmonary Medicine, University of Utah Spencer Fox Eccles School of Medicine, Salt Lake City, UT; †George E. Wahlen Department of Veterans Affairs Medical Center, Salt Lake City, UT; and ‡Pharmacology and Toxicology, College of Pharmacy, University of Utah, Salt Lake City, UT

ORCIDs: 0009-0004-5425-7511 (E.Z.); 0000-0002-5006-1982 (C.A.R.); 0000-0003-0680-4037 (K.W.); 0000-0002-0536-4175 (M.A.Z.); 0000-0002-0954-8481 (M.N.H.).

Received for publication May 11, 2023. Accepted for publication June 17, 2024.

This work was supported by U.S. Department of Veterans Affairs Merit Grant 5I01BX001777 awarded to R.P.

Address correspondence and reprint requests to Dr. My N. Helms and Robert Paine III, University of Utah, 50 Medical Drive, Salt Lake City, UT 84132 (M.N.H.); and University of Utah, 30 North Mario Capecchi Drive, 2nd Floor North, Salt Lake City, UT 84132 (R.P.). E-mail addresses: my.helms@hsc.utah.edu (M.N.H.) and robert.paine@hsc.utah.edu (R.P.)

Abbreviations used in this article: AEC, alveolar epithelial cell; αSMA, α-smooth muscle actin; ATCC, American Type Culture Collection; BALF, BAL fluid; AHR, aryl hydrocarbon receptor; EMT, epithelial–mesenchymal transition; KD, knockdown; PAH, polycyclic aromatic hydrocarbons; TEER, transepithelial electrical resistance.

https://doi.org/10.4049/jimmunol.2300325

Materials and Methods

Animals

Adult (5–12 wk old) male wild-type C57BL/6 mice [RRID:IMSR_JAX:000664] were obtained from The Jackson Laboratory (Bar Harbor, ME) and used in accordance with the National Institutes of Health guidelines for the care and use of laboratory animals. All studies were approved by the institutional animal care and use committee of the U.S. Department of Veterans Affairs located in Salt Lake City, UT. Mice were housed under specific pathogen-free conditions under a normal light/dark cycle, given ad libitum access to food and water, and monitored daily by veterinary staff. Ambient temperature was maintained between 22.2°C and 23.3°C in the U.S. Department of Veterans Affairs vivarium. Following treatment, mice were anesthetized with an i.p. injection of 0.015 ml/g Avertin (Sigma-Aldrich, St. Louis, MO) and heparin at 0.05 ml/injection and then exsanguinated. Mice were randomly selected for treatment groups.

Tissue culture

Primary mouse AECs were isolated on the basis of methods described in our prior work (12–15). AECs were plated on fibronectin-coated tissue culture dishes coated with human fibronectin (Millipore, Burlington, MA) at 50 μg/ml in PBS and cultured in modified HITES medium (formulated by American Type Culture Collection [ATCC], Manassas, VA, as follows: DMEM/Ham F12 50:50 mix [catalog no. 30-2006]) supplemented with 10% FCS in an atmosphere of ambient air with 5% CO_2 at 37°C for 3 d prior to experimentation. Primary cells were cultured for 48 h prior to experimentation, unless otherwise noted in the time-course study. Low-passage immortalized mouse MLE-15 cells [RRID:CVCL_D581] were a gift from Dr. J. Whitsett (Cincinnati Children's Hospital Medical Center, Cincinnati, OH). MLE-15 cells are SV40 transformed murine alveolar type II cells commonly used to study the regulation of alveolar epithelial genes and to model epithelial cell differentiation (16). AECs and MLE-15 cells were rinsed three times with PBS prior to drug treatments prepared in HITES media, as indicated in the figure legends. Low-passage human Calu-3 human lung bronchial epithelial cells (ATCC HTB-55, RRID:CVCL_0609) were purchased from ATCC. Calu-3 cells were cultured in Eagle's MEM supplemented with 10% FBS, 1% penicillin and streptomycin, 1% nonessential amino acids, and 1% sodium pyruvate in a humidified incubator with 5% CO_2 at 37°C. Primary human small airway epithelial cells were purchased from Lonza (catalog no. CC-2547; 66-y-old Caucasian female_18TL075838) and cultured in SAGM Small Airway Epithelial Cell Growth Medium SingleQuots Supplements and Grown Factors (catalog no. CC-4124).

AHR ligands

A standardized mixture of polycyclic aromatic hydrocarbons (PAH; 2 mg/ml in methylene chloride) was supplied by Restek (Bellefonte, PA; catalog no. 31011, calibration mix 5/610 PAH). The following compounds are included in the PAH mix: acenaphthene (83-32-9); acenaphthylene (208-96-8); anthracene (120-12-7); benz(a)anthracene (56–55-3); benzo(a)pyrene (50–32-8); benzo(b)fluoranthene (205-99-2); benzo(k)fluoranthene (207-08-9); benzo (ghi)perylene (191-24-2); chrysene (218-01-9); dibenz(a, h)anthracene (53-70-3); fluoranthene (206-44-0); fluorene (86-73-7); indeno(1,2,3-cd) pyrene (193-39-5); naphthalene (91-20-3); phenanthrene (85-01-8); pyrene (129-00-0). Prior to use, the solvent in PAH mix was removed via evaporation and followed by reconstitution in tissue culture grade DMSO (1 μg/ml) and storage at −80°C.

Benzo(a)pyrene (BaP; CAS number 50-32-8) and pyrene (CAS number 129-00-0) were obtained from Sigma-Aldrich. FICZ (5,11-dihydroindolo [3,2-*b*] carbazole-6-carboxaldehyde; CAS number 172922-91-7) was purchased from Tocris Bioscience (Bristol, UK). Chemical compounds were solubilized in tissue culture grade DMSO. Final working concentrations of AHR agonists were prepared immediately prior to experimentation in HITES media with minimal concentrations of DMSO (≤0.1%). Vehicle control treatments consisted of 0.1% DMSO in HITES media.

Real-time PCR

Total cellular RNA was isolated using the Quick RNA Mini-Prep kit (Zymo Research, Irvine, CA) and first-strand cDNA synthesis was conducted using High-Capacity cDNA Reverse Transcription (Applied Biosystems/Thermo Scientific, Waltham, MA). Real time (RT)-PCR was carried out using PowerUp SYBR Green Master Mix and a StepOnePlus system (Applied Biosystems/Thermo Scientific). Primers were designed using NIH Primer-BLAST and Roche Universal Probe Library, then synthesized at the University of Utah DNA/Peptide Synthesis Core Facility (Salt Lake City, UT). The mouse primer pair sequences used to amplify the respective genes were as follows: Ahr: 5′-ACCAGAACTGTGAGGGTTGG-3′ (forward) and 5′-TCTGAGGT GCCTGAACTCCT-3′ (reverse); Cyp1a1: 5′-TCTTTTGGGAGGAAGTGG-AATAGACACTGATCTGGCTGCAG-3′ (forward) and 5′-GGGAAGGCTC-CATCAGCATC-3′ (reverse); Il-6: 5′-TGATGGATGCTACCAAACTGG-3′ (forward) and 5′-TCCATGTACTCCAGGAGGTAGCTATGG-3′ (reverse); Mcp-1: 5′-CATCCACGTGTTGGCTCA-3′ (forward) and 5′-GATCATCTT GCTGGTGAATGAGT-3′ (reverse); αSma: 5′-GACACCACCCACCCAG AGT-3′ (forward) and 5′-ACATAGCTGGAGCAGCGTCT-3′ (reverse); Col1a1: 5′-CATGTTCAGCTTTGTGGACCT-3′ (forward) and 5′-GCAGCT GACTTGAGGGATGT-3′ (reverse); Fn1: 5′-CGGAGAGAGTGCCC TACTA-3′ (forward) and 5′-CGATATTGGTGAATCGCAGA-3′ (reverse); E-Cdh1: 5′-AAGTGACCGATGATGATGCC-3′ (forward) and 5′-CTTCT CTGTCCATCTCAGCG-3′ (reverse); Col4A1: 5′-GGCCCTTCATTAGCA GGTG-3′ (forward) and 5′-TCTGAATGGTCTGACTGTGTACC-3′ (reverse); Sdc 1: 5′-GAGGGCTCTGGAGAACAAGA-3′ (forward) and 5′-TGTGGCT-CCTTCGTCCAC-3′ (reverse); Nqo1: 5′-TATCCTTCCGAGTCATCTC-TAGCA-3′ (forward) and 5′-TCTGCAGCTTCCAGCTTCTTG-3′ (reverse); Ahrr: 5′-GAGAGTGTACATACGCCGGT-3′ (forward) and 5′-GCTCT-GTATTGAGGCGGTCC-3′ (reverse).

The above primers were used for amplification using the StepOnePlus machine's FAST protocol (50°C for 2 min, 95°C for 2 min, and 40 cycles of 95°C for 15 s, 60°C for 1 min). ΔCt was calculated using target gene Ct values normalized to a housekeeping gene (*β-actin*). Data are expressed as fold change ($2^{-\Delta\Delta Ct}$) over average control values.

ELISA

Expression of inflammatory cytokines (IL-6, MCP-1, TNF-α, and CXCL2) in cell-free culture supernatants were determined using DuoSet kits following the manufacturer's protocol (R&D Systems Bio-Techne, Centennial, CO). In each experiment, media were collected, immediately centrifuged to remove cell debris, and either immediately assayed for cytokines levels by ELISA or stored at −80°C for subsequent assay. AHR detection from whole-cell proteins extracted from cells in culture was performed using a commercially available AHR ELISA kit (Novus Biological, Bio-Techne, Centennial, CO). Total protein concentration was determined by standard BCA protein assay (Pierce Biotechnology, Waltham, MA).

Western blot analysis

After treatment, cells were washed with ice-cold PBS supplemented with 1× Halt protease and phosphatase inhibitor mixture (Thermo Fisher). Cells were lysed in ice-cold buffer containing 1% Nonidet P-40, 0.5% deoxycholic acid, 0.1% $NaDodSO_4$ (SDS), 10% sucrose, Halt inhibitor mixture, 1 mM PMSF, 0.25 mM DTT, and 14.25 mM 2-ME. Standard SDS-PAGE and immunoblotting techniques were used. Briefly, 10–20 μg protein lysates were electrophoresed on a 4–15% gradient acrylamide gel (Bio-Rad Laboratories, Hercules, CA) and then transferred to 0.2-μm polyvinylidene difluoride membrane and then immunoblotted with rabbit monoclonal anti-mouse AHR (Thermo Fisher Scientific, catalog no. MA5-47249, RRID:AB_2938321) at 1:200 overnight with agitation at 4°C. To detect immunoreactive signal on Western blot analysis, polyvinylidene difluoride membranes were incubated in 1:2500 secondary Ab (Thermo Fisher, catalog no. 32460, RRID:AB_1185567) at room temperature for 1 h. Luminescent signal was detected using SuperSignal West Femto substrate (Thermo Fisher) and analyzed on an Amersham 680 gel documentation system with compatible ImageQuant software (Cytiva Life Sciences, Marlborough, MA). Signal intensity was normalized to sample loading, determined by HRP-conjugated mouse β-actin (Abcam, Catalog no. ab49900, RRID:AB_867494) for 1 h at 1:20,000. All signal intensities were scored by an experimenter blinded to protein identity.

Lentiviral shRNA

Knockdown (KD) of the *Ahr* gene in primary murine AECs was achieved by transducing the cells with *Ahr* shRNA lentiviral particles supplied by Sigma-Aldrich. Forty-eight hours after isolation, AECs were washed with PBS and supplied fresh media containing 8 μg/ml polybrene and lentiviral transduction particles at a multiplicity of infection of 18:1, according to confluence. AECs were incubated with lentiviral particles and polybrene for 48 h, then rinsed with PBS and incubated an additional 12 h in fresh media before collection for RNA or whole-cell protein extract.

CRISPR-Cas9

CRISPR-Cas9 was used to introduce mutations into the murine *Ahr* gene in MLE-15 cells. The University of Utah Mutation Generation and Detection Core (Salt Lake City, UT) identified optimal CRISPR-Cas9 target sites for the murine *Ahr* gene on exon 1 (2669) and exon 2 (2670) and supplied sequence confirmed plasmids for transduction using Lipofectamine 3000 (Thermo Fisher). Two rounds of puromycin antibiotic selection (2 μg/ml) were used to select transfected cells. Cloning disks were used to expand surviving MLE-15 cells, and positive clones were identified on the basis of a lack of

AHR transcripts and lack of induction of AHR inducible genes, as well as lower AHR protein expression.

CYP1A1 activity (p450GLO)

P450-CYP1A1 functional activity was measured in MLE-15 wild-type, CRISPR control, and *Ahr* knockout clones using the P450-Glo CYP1A1 Assay System (Promega, Madison, WI; catalog no. V8752) per the manufacturer's protocol and as described in (17).

In vitro scratch wound assays

MLE-15 clones were plated at 25,000 cells/cm^2 and grown to 100% confluence on gridded 96-well culture plates (Incucyte ImageLock, Essen BioScience, Ann Arbor, MI). Following a "scratch" made by an IncuCyte WoundMaker (96-pin wound-making tool, Essen BioScience), the cells were washed twice with PBS to remove detached cells, and treatments were applied (as indicated in the figures). The scratch wound closure images were captured at hourly intervals using the IncuCyte incubator-located microscope and compatible IncuCyte Zoom software. Kinetic gap closure analysis (gap width and cell covered area change over time) was conducted and interpreted to represent cellular wound healing using the Scratch Wound analysis of the IncuCyte ZOOM software.

Transepithelial electrical resistance (TEER) and barrier integrity

Murine AECs, isolated according to the protocol above, were seeded at 5×10^5 cells per 0.4-μm Transwell insert (Corning Costar, Corning, NY) coated with fibronectin and under liquid/liquid interface (18). Twenty-four hours after seeding, cells were rinsed with PBS to remove any dead cells or RBCs. Following rinse, fresh media were added to the basal chamber and the apical chamber was left empty to establish an air–liquid interface cell culture. Vehicle control, FICZ, or LPS was added to basal media (as indicated in figure legends) to assess the effects on barrier formation, and cells were kept cultured in air–liquid interface conditions, with cells rinsed and media changed every other day until a monolayer was formed. Upon visual confluence of ~90%, media were added to the apical chamber at media change to allow TEER measurements, using a Millicell ERS Voltohmmeter (MilliporeSigma, Burlington, MA), beginning after cell cultures were resubmerged for 24 h. TEER was measured at regular intervals until EVOM values for all treatments had plateaued. Cell barrier integrity was assessed by challenging cells that had reached plateaued TEER values with mouse TNF-α (100 μg/ml) (R&D Systems) and mouse IFN-γ (100 μg/ml) (BioLegend, San Diego, CA) in addition to the vehicle control or FICZ as before. TEER values were measured starting immediately following the addition of treatment and at time points (as indicated in the figure legend) throughout the 9-h challenge.

Biomolecular assays and acute lung injury

To determine whether FICZ instillation into the lung alleviates LPS-induced acute lung injury and inflammation, adult male C57BL/6 mice were intranasally instilled with a single dose of LPS as described in (19), a single dose of FICZ as described in (20, 21), or both LPS and FICZ ($n = 5$ per group). To accomplish this, a solution containing 0.14 mM FICZ and/or 0.40 μg/μl LPS was prepared in sterile PBS and nasally instilled at a volume of 0.8 μl/g body weight for a total of 1 μg FICZ and/or 10 μg LPS administration per 31.25-g mouse. Control mice were inoculated with an equal volume of 0.1% DMSO in PBS. The mice were euthanized 18 h after nasal instillation, and the lungs were lavaged with Ca^{2+}/Mg^{2+}-free PBS containing 0.5 mM EDTA. Unperfused lungs were removed en bloc, minced, and then partitioned into RNAlater (Invitrogen) or snap-frozen in a dry ice/methanol bath for subsequent biomolecular analysis. Lung tissue stored in RNAlater was subsequently homogenized in RNA lysis buffer (100 mg/ml; Zymo), passed through a QIAshredder (Qiagen, Hilden, Germany), and processed for RT-PCR.

BAL fluid (BALF) cells were collected, and a differential Wright stain was performed on 1×10^5 cells following cytospin. The remainder of BALF cells were resuspended in RNA lysis buffer and processed as described above for RT-PCR analysis. The inflammatory cytokine level of the cleared BALF was determined by ELISA (R&D Systems DuoSet ELISA kits for IL-1β; TNF-α; and CXCL2). Protein content of cleared BALF was measured using a standard BCA protein assay (Pierce Biotechnology).

Snap-frozen lung tissue was homogenized in Tissue Extraction Buffer 1 (100 mg/ml; Invitrogen) containing HALT protease inhibitors (Thermo Scientific). After homogenization, the extract was sonicated, then cleared by centrifugation. The protein content of the cleared supernatant was measured using a standard BCA assay, and the amount of inflammatory cytokines was determined by ELISA.

Statistical analysis

Data are presented as mean ± SEM. Statistical analysis was carried out using GraphPad Prism version 4C software (GraphPad Software). Two-tailed tests of significance were used to compare two groups. Differences between multiple groups were compared with one-way ANOVA followed by Tukey post hoc test. Comparisons were deemed statistically significant for p values <0.05. Biological and technical replicates are indicated in the figure legends.

Results

Canonical AHR signaling in primary murine AEC

In Western blot analysis of whole-cell extracts of unstimulated murine (MLE-15 and primary AECs) epithelial cells, AHR protein is found near the 100 kDa molecular mass indicator (Fig. 1A). For reference, we also show AHR protein in human (Calu-3 and human small airway epithelial cells) lung epithelial cells. Following stimulation with the endogenous AHR ligand, FICZ, the classic AHR pathway target genes, *Cyp1a1* and *Ahrr*, are induced (Fig. 1B). These data indicate that functional AHR signaling in primary murine AECs initiates transcription of detoxifying enzymes (i.e., CYP1A1) and is capable of controlling expression of its own repressor protein (AHRR), as expected in the canonical AHR signaling pathway. Moreover, exposure of primary murine AECs to a variety of endogenous and exogenous AHR ligands (such as PAH, FICZ, or BAP) results in induction of classical AHR-activated genes *Cyp1a1* and *Nqo1* (Fig. 1C, 1D). In contrast, pyrene, a PAH that has low binding affinity for AHR (22, 23), failed to induce these genes. Together these data confirm that AHR is present and active in AECs, with stimulation resulting in canonical AHR pathway signaling.

AHR activation attenuates LPS-stimulated cytokine release in AECs and MLE 15 lung epithelial cells in vitro

AECs play a critical role as sentinel cells, releasing key early response inflammatory mediators (especially TNF, IL-6, and CXCL2) in response to inflammatory stimuli such as LPS (24–26). Interestingly, LPS-mediated expression of TNF-α, IL-1β, and CXCL2 in primary murine AECs was significantly reduced by treatment with the endogenous AHR ligand, FICZ (Fig. 2A–2C). These data affirm AHR's anti-inflammatory role in primary AECs. Similarly, in the MLE-15 cell line, TNF-α induction of *Il-6* and *Mcp-1* was also suppressed by FICZ (Fig. 2D–2F).

Activation of AHR with FICZ limits lung injury and inflammation in a mouse lung injury model

We extended these observations concerning the potential role of AHR activation in suppression of acute inflammation to a murine model of acute lung injury. Mice were inoculated intranasally with 10 μg LPS with or without coadministration of 1 μg FICZ. FICZ treatment (with or without LPS) was associated with activation of AHR, as indicated by induction of *Cyp1a1* mRNA expression in whole-lung homogenates (Fig. 3A). As anticipated, inoculation with LPS induced inflammatory lung injury, with significant protein leak and BAL neutrophil accumulation and cytokine protein expression. Administration of FICZ to mice challenged with LPS significantly reduced protein leak into the BALF (Fig. 3B) and was associated with reduced neutrophil predominance in BALF (Fig. 3C). Coadministration of FICZ and LPS also significantly decreased LPS-induced release of IL-1β, TNF-α, and CXCL2 protein (Fig. 3D–3F). This anti-inflammatory effect was also demonstrated in an assay of lung homogenate studies (Fig. 3G–3I).

AHR activation suppresses induction of EMT genes in AECs in vitro

It is clear that proinflammatory processes may be associated with EMT, with important implications for organ physiology and cancer

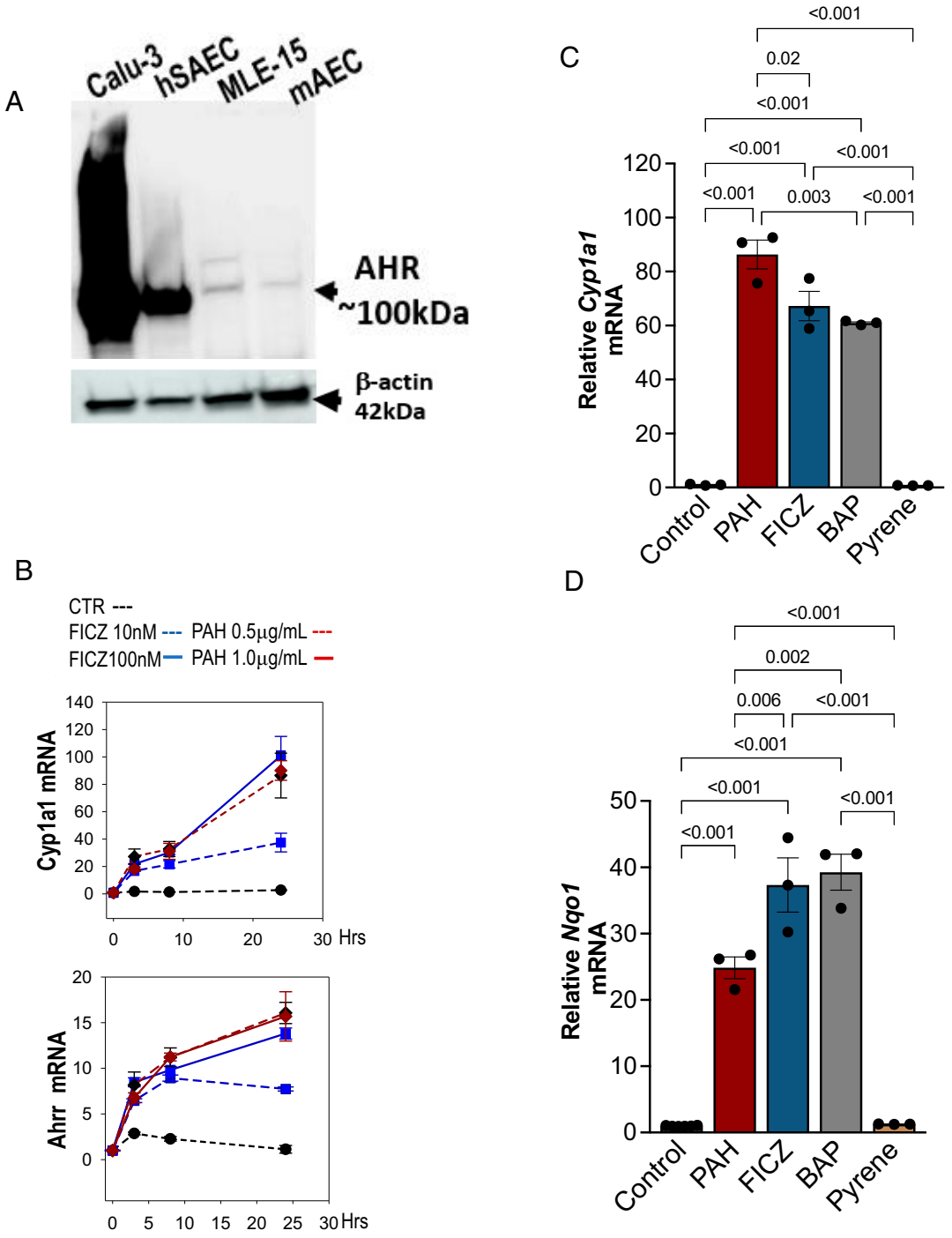

FIGURE 1. Functional AHR expression in murine AECs. (**A**) Top panel: 12 μg human (lanes 1 and 2) and mouse (lanes 3 and 4) whole-cell extracts separated on SDS-PAGE gel and blotted with RRID:AB_2938321 for AHR protein expression. (**B**) Top panel: time course of *Cyp1a1* expression in MLE-15 cells following FICZ (blue lines) and PAH (red lines) stimulation. Bottom panel: time course of *Ahrr* expression following FICZ and PAH stimulation; $n = 3$ with mean values plotted. (**C**) *Cyp1a1* and (**D**) *Nqo1* mRNA transcript levels following control, PAH (1 μg/ml), FICZ (100 nM), BaP (10 μM), or pyrene (10 μM) exposure for 24 h. Data are representative of three independent experiments; statistical evaluation was conducted with ANOVA followed by Tukey post hoc test.

progression (27, 28). To better understand whether AHR plays a role in mitigating EMT in lung epithelia, AECs and MLE-15 cells were treated with TGF-β in the presence or absence of FICZ. TGF-β is a key driver of EMT and fibrosis in human lung epithelia (29, 30). Treatment with FICZ suppressed the expression of the classic EMT marker, α-smooth muscle actin (αSMA), in response to TGF-β stimulation, both in primary murine AECs (Fig. 4A) and in MLE-15 cells (Fig. 4B). Thus, these data suggest a potential role of AHR activation in maintaining epithelial cell phenotype in the face of transitional pressure. To further explore this, we evaluated mesenchymal and epithelial cell markers following shRNA and CRISPR-Cas9 KD of *Ahr* below.

AHR activity plays an important role in epithelial cell integrity

Ahr gene expression in primary AECs was knocked down using an shAHR lentivirus construct. Fig. 5A shows that transduction with

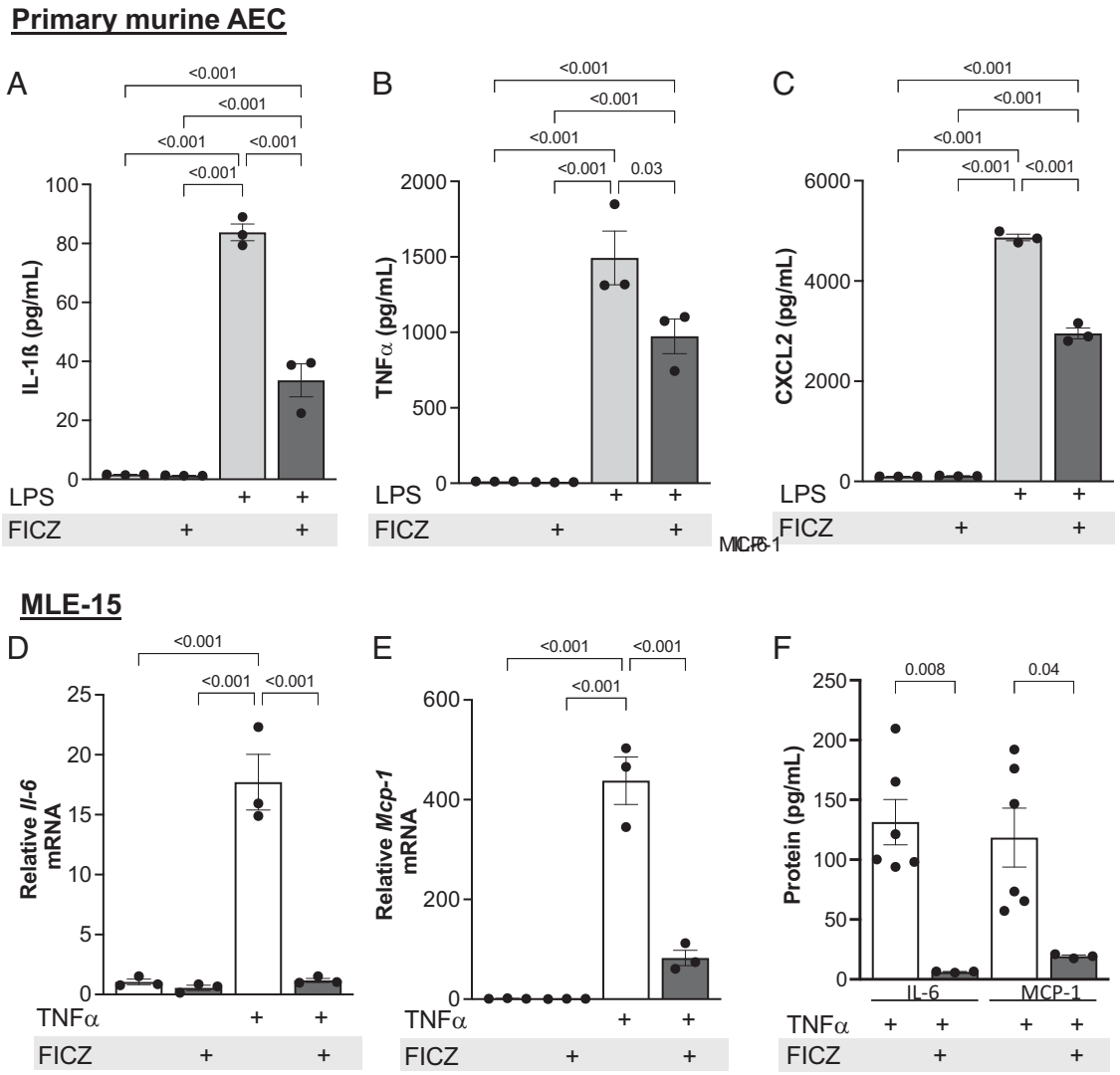

FIGURE 2. FICZ ligand activation of AHR attenuates LPS-stimulated cytokine release in lung epithelia. AECs were exposed to 0.1% DMSO (vehicle control), FICZ (100 nM), LPS (100 ng/ml), or a combination of FICZ (100 nM) and LPS (100 ng/ml) for 24 h. Inflammatory cytokines (**A**) IL-1β, (**B**) TNF-α, and (**C**) CXCL2 were measured in the culture supernatants by ELISA. (**D** and **E**) MLE-15 cells were stimulated with TNF-α (5 ng/ml) in the presence or absence of FICZ (100 nM) for 24 h. (D) *Il-6* and (E) *Mcp-1* mRNAs were measured in cell lysates and (**F**) IL-6 and MCP-1 proteins were measured in culture supernatants by ELISA. Data are representative of three independent experiments; multiple comparison analysis was conducted using ANOVA followed by Tukey post hoc test.

this lentiviral construct results in decreased AHR protein expression as determined by Western blot analysis with Abs directed against the C-terminus of mouse AHR. This KD is associated with upregulation of the mesenchymal genes α*Sma*, *Col1a1*, and *Fn1* (Fig. 5B). Conversely, the expression of epithelial gene *Col4a1* and cell–cell interaction gene *Sdc1* were significantly decreased in AHR KD AECs, although expression of the pan-epithelial marker E-cdh1 was not altered.

An alternative KD strategy using CRISPR-Cas9 in the MLE-15 cell line was used to further investigate the hypothesis that ligand-activated AHR plays an important role in maintaining epithelial cell integrity. Control MLE-15 cells transduced with a nonspecific scrambled CRISPR-Cas9 sequence that does not exist in nature served as the experimental CRISPR control cell line. Deletion of *Ahr* in three knockout clones (two clones using construct 2669 [33-1 and 33-2] and one with construct 2670 [49-1]) resulted in decreased AHR protein expression (Fig. 5C); reprobing the nitrocellulose membrane for β-actin (42 kDa) confirms equal protein loading. Quantification of CRISPR downregulation of AHR (normalized to β-actin) is shown in Fig. 5Ci–5Ciii and is validated with ELISA analysis of AHR protein levels using plates precoated with Abs directed against the N-terminus of mouse AHR (Fig. 5D). As anticipated, these AHR KD clones fail to respond to both endogenous and exogenous ligands, as indicated by suppressed *Cyp1aA1* mRNA induction compared with CRISPR controls (Fig. 5E). Finally, in these CRISPR-Cas9 KD clones, loss of functional *Ahr* expression significantly upregulates αSma gene expression and significantly decreases *Col4a1* and *Sdc1* gene expression (Fig. 5F–5H). Together, these data using different approaches to *Ahr* KD demonstrate that AHR works to restrict baseline expression of genes associated with EMT in murine AECs.

AHR plays an important role in maintenance of epithelial cell physiologic characteristics

EMT may both contribute to and detract from epithelial defense, depending on the cellular context (31). In the setting of epithelial injury, a potentially beneficial effect of EMT is the promotion of more rapid migration of cells to cover a wounded area (32). However, expression of mesenchymal characteristics at the expense of fully differentiated epithelial characteristics may result in scar formation and impaired epithelial function (33). To assess this dichotomy, we have

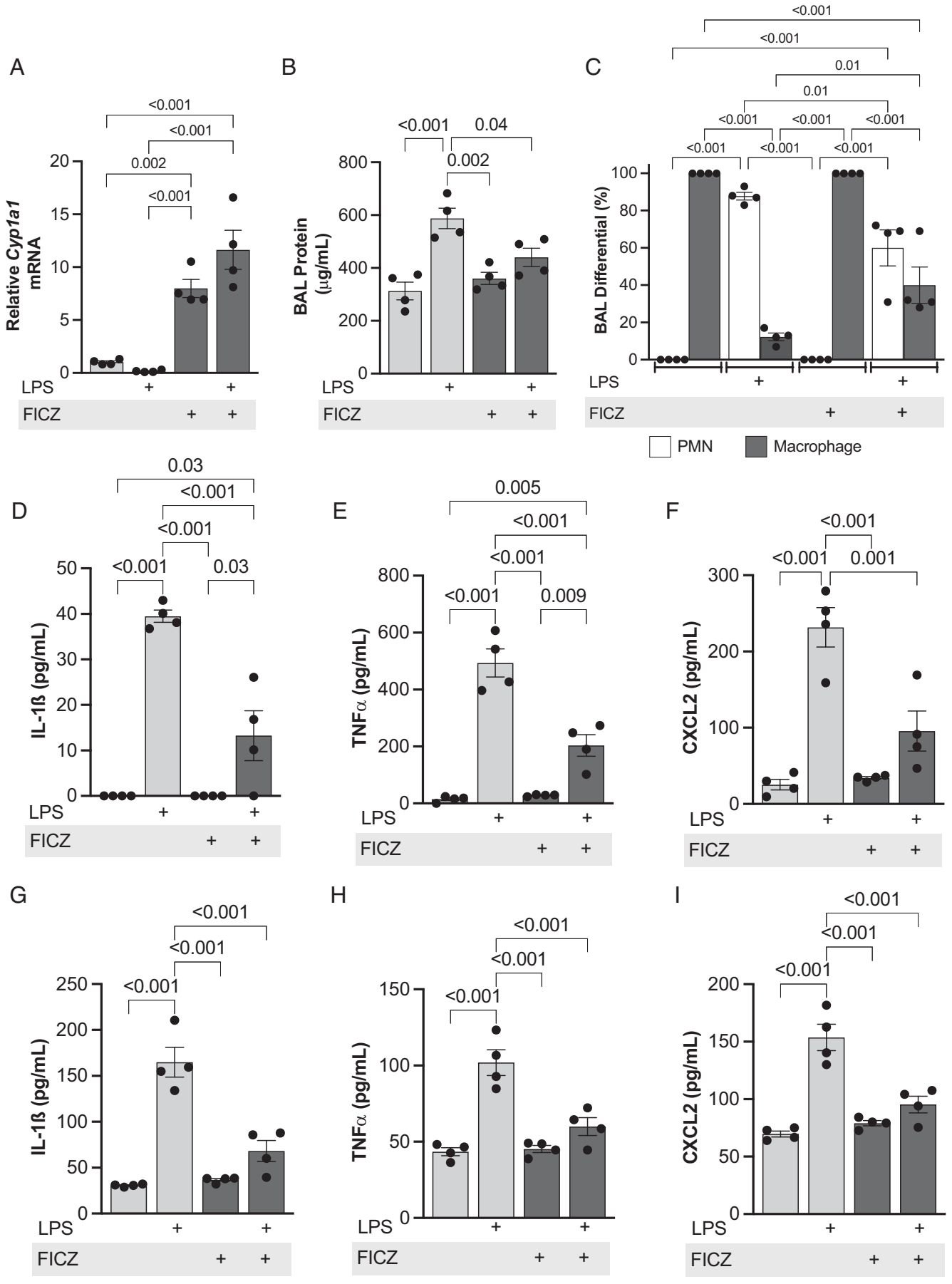

FIGURE 3. Lung-directed treatment with FICZ reduces protein leak and inflammation while limiting induction of αSMA in a murine LPS-induced acute lung injury model. (**A–C**) Mice were given LPS (10 μg/mouse, intranasally [IN]) with or without concurrent FICZ (1 μg/mouse, IN). Controls *(Figure legend continues)*

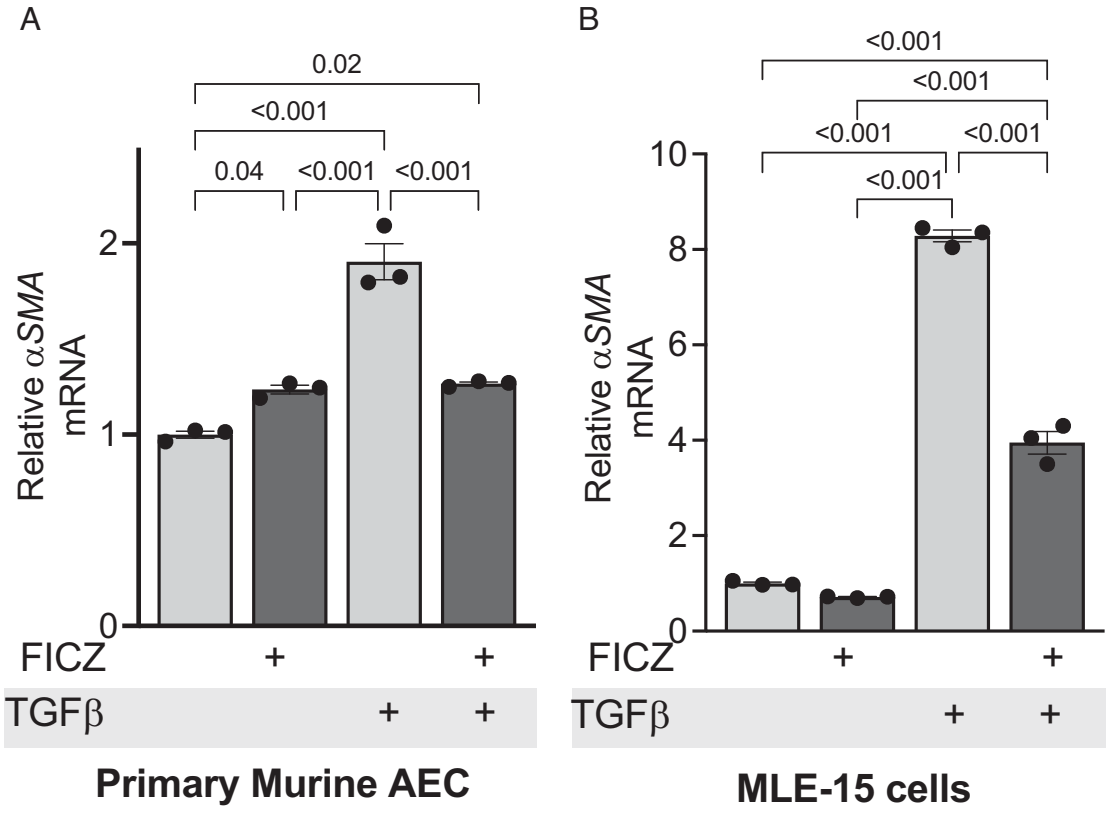

FIGURE 4. FICZ attenuates TGF-β–mediated increase in αSma expression. (**A**) Primary murine AECs and (**B**) MLE-15 cells were cultured for 3 d before treatment with TGF-β1 (10 ng/ml) with or without FICZ 100 nM for 24 h. Vehicle = 0.1% DMSO prepared in media. Data are representative of three independent experiments; multiple comparison analysis was conducted using ANOVA followed by Tukey post hoc test.

separately evaluated the effects of AHR activation on wound closure as a manifestation of the former (Fig. 6) and on barrier function (i.e., TEER measurements) as a reflection of the latter (Fig. 7).

To assess the effect of AHR on wound closure, wild-type MLE-15, CRISPR control MLE-15, and CRISPR *Ahr* KD MLE-15 cells were studied in a scratch wound healing assay over the course of 45 h. *Ahr* KD resulted in accelerated wound closure compared with either untreated wild-type or CRISPR control MLE-15 cells (Fig. 6A, 6B). In a related study, we assessed the rate of wound closure in wild-type MLE-15 cells treated with vehicle control (DMSO), FICZ, PAH, or BaP. We found that ligand-induced activation of AHR helping to maintain a less motile epithelial cell phenotype (Fig. 6C). These data suggest a role of endogenous AHR activity in suppressing characteristics associated with EMT.

To assess the impact of AHR activation on epithelial cell barrier function, primary AECs were maintained in culture in the presence or absence of FICZ (100 nM). Treatment with FICZ resulted in a tighter monolayer (as indicated by greater TEER values) versus untreated control primary cells maintained under similar conditions (Fig. 7A). As expected, treating AECs with inflammatory cytokines (TNF-α and IFN-γ) disrupted barrier function, leading to decreased TEER measurements. Interestingly, however, this decrease in TEER was significantly reduced by treatment with FICZ (Fig. 7B). Thus, activation of AHR enhanced barrier characteristics of primary murine AECs and limited barrier dysfunction induced by inflammatory cytokines.

Limitation of inflammation-induced mesenchymal gene expression by FICZ ligand activation of AHR in vivo

It has been reported previously that LPS induces EMT via NF-κB–mediated signaling (34, 35). Therefore, we extended our observations of the effects of FICZ treatment on lung epithelial cell integrity to our murine model of acute lung injury in response to LPS. Mice were inoculated intranasally with 10 μg LPS with or without coadministration of 1 μg FICZ, and αSma mRNA expression was determined in the lung homogenates. Fig. 8 shows that exposure to LPS led to increased expression of αSma and that treatment with FICZ suppressed this induction of αSma. These data extend our findings in Fig. 3. Together, Figs. 3 and 8 show that activation of AHR with FICZ can limit inflammatory stress induced by intratracheal inoculation with LPS in C57BL/6 mice.

Discussion

AHR is widely expressed across species and tissues. Since its discovery, there has been considerable focus on its role as a receptor for environmental toxicants (36), triggering transcription of a large collection of genes, including cytochrome P450 genes such as *CYP1A1*

received an equivalent volume of 0.1% DMSO in PBS. BALF and lung homogenate were collected 18 h after treatment to assess (A) *Cyp1a1* mRNA induction in lung homogenate, (B) protein concentration in BALF, and (C) cell differential in BALF. Data are representative of three independent experiments; $n = 4$. Inflammatory cytokines were measured by ELISA in BAL (**D**–**F**) and in lung homogenate (**G**–**I**). (D and G) IL-1β, (E and H) TNF-α, and (F and I) CXCL2 protein levels were determined in LPS-treated mice with or without FICZ. Data are representative of three independent experiments; multiple comparison analysis was conducted using ANOVA followed by Tukey post hoc test.

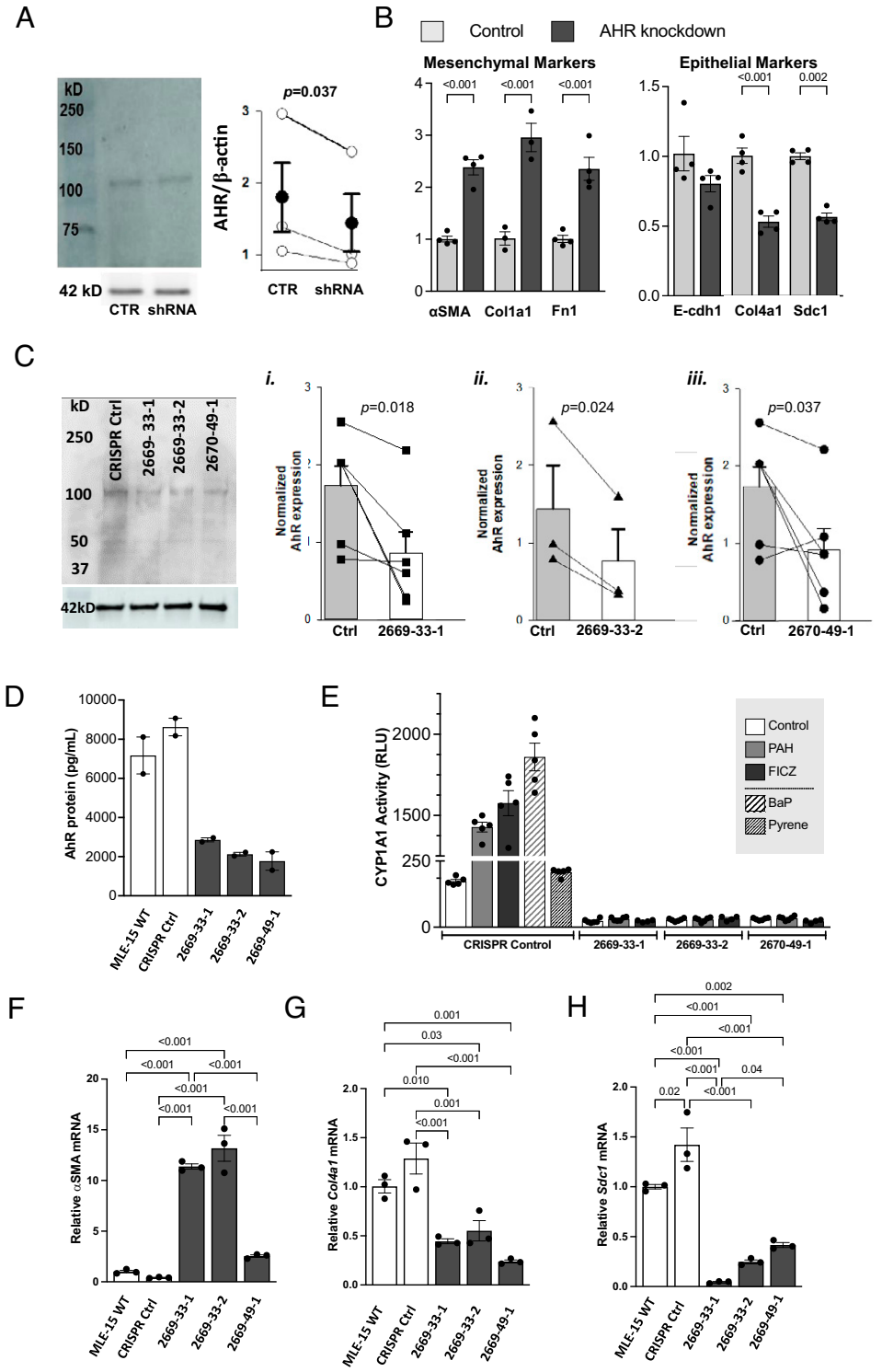

FIGURE 5. AHR KD modulates epithelial cell integrity. (**A**) Western blot confirmation of lentiviral shRNA KD of AHR protein in primary murine AECs using a 1:200 dilution of RRID:AB_2938321 Ab. The *t* test indicates $p = 0.03$. (**B**) RT-PCR measurement of mesenchymal (left panel) and epithelial cell markers (right panel) of control AECs versus shRNA KD of AHR in AECs. Data shown are representative of two independent experiments with replicates as shown. Statistical evaluation was conducted using a *t* test, with *p* values indicated. (**C**) Western blot confirmation of CRISPR-Cas9 KD of AHR activity in MLE-15 cells; densitometric quantification of clones is shown in panels (i)–(iii). Pairwise comparisons were conducted with a *t* test; $p < 0.05$ as indicated. (**D**) ELISA validation of AHR protein levels in whole-cell extracts from wild-type MLE-15 cells, Crispr-Cas9 cloned nontargeting (2082) control cells, and three CRISPR-Cas9 AHR target-specific clones (2669-33-1, 2669-33-2, and 2670-49-1); two extractions per cell type. (**E**) CYP1A1 activity was measured following 24-h exposure to PAH (1 μg/ml), FICZ (100 nM), BaP (10 μM), or pyrene (10 μM). RLU, relative light units; $n = 3$. The expression of (**F**–**H**) *aSma*, *Col4a1*, and *Sdc1* mRNA is shown in control and CRISPR-Cas9 AHR KD MLE-15 clones; $n = 3$; multiple comparison analysis was conducted using ANOVA followed by Tukey post hoc test, with *p* values indicated.

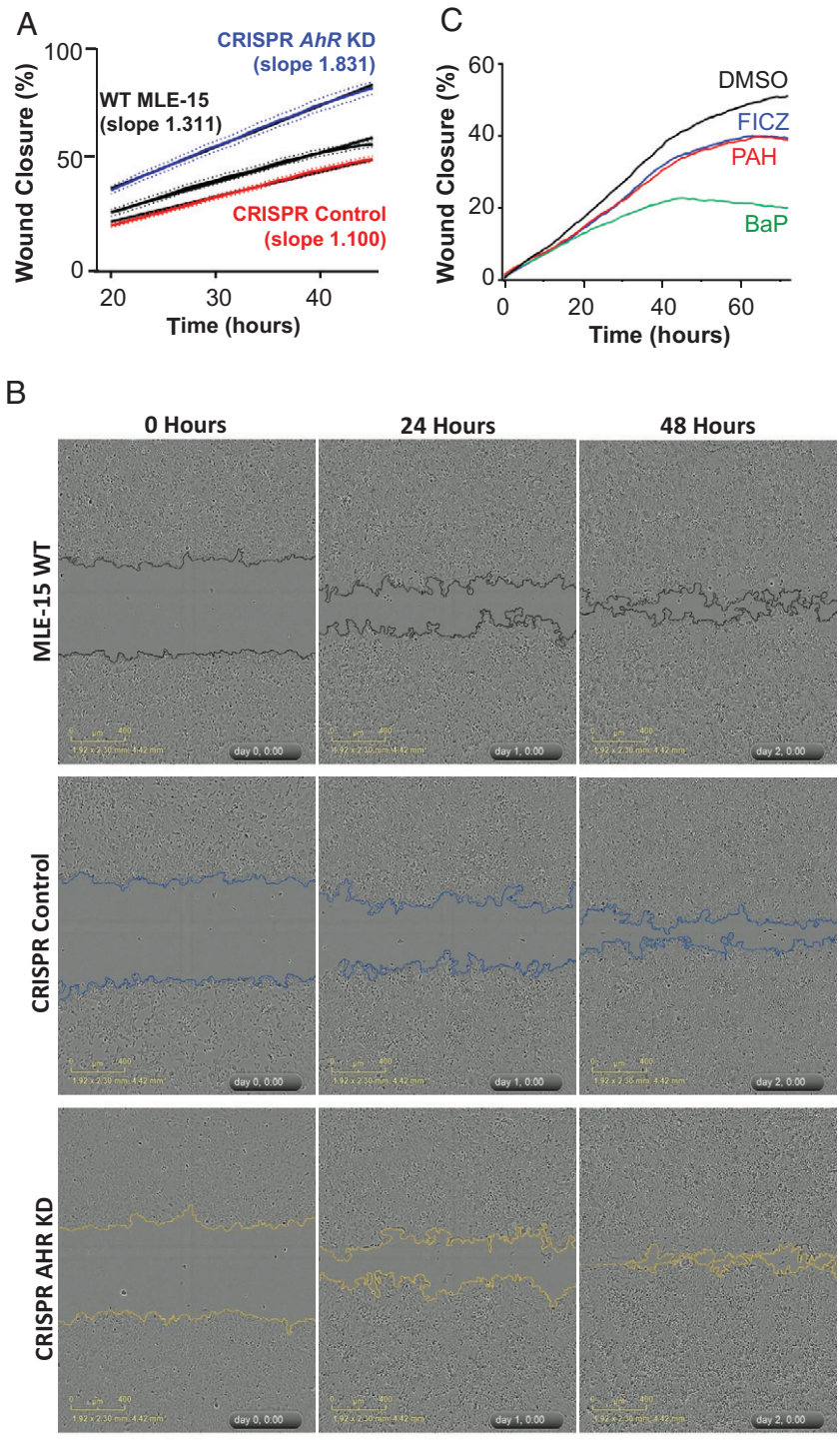

FIGURE 6. AHR modulates epithelial cell wound closure. (**A**) The effect of AHR KD on MLE-15 cell wound closure over 48 h in a scratch model. The slope of the percentage wound confluence (representative of three individual experiments) is shown. (**B**) Representative images of the control and AHR monolayers at day 1 and day 2. Scale bar, 400 μm; dashed outlines indicate the areas used for quantification. A time-lapse video of wound recovery can be viewed in a supplemental file: https://doi.org/10.6084/m9.figshare.25343233. (**C**) The effect of AHR ligands PAH (1 μg/ml), BaP (10 μM), and FICZ (100 ng/ml) on wound closure in MLE-15 cells with intact AHR signaling (CRISPR control) cell wound closure. Data are representative of three independent experiments.

and *CYP1B1*. However, the evolutionary conservation and extensive expression of AHR has argued for roles for this receptor beyond the response to manmade environmental toxicants. A number of endogenous ligands for AHR have been identified, including products of tryptophan metabolism (37–39). Data have now emerged describing a range of activities of these ligand–receptor interactions, implicating AHR in development, host defense, epithelial integrity, and wound healing (40).

In this work, we report the effects of ligand-stimulated AHR activation in lung AECs. Salient points include the following: (1) In the setting of stimulation with the endogenous AHR ligand, FICZ, lung epithelial expression of innate immune molecules in response to inflammatory stimulation was significantly suppressed. (2) At the same time, treatment with FICZ limited TGF-β–stimulated induction of molecules and physiologic characteristics associated with EMT. (3) Conversely, we found that AHR KD using different genetic approaches in primary AECs and MLE-15 cells was associated with enhanced expression of mesenchymal characteristics in these epithelial cells, demonstrating a homeostatic role of AHR in preserving epithelial integrity. (4) Finally, we extended our observations to the intact lung in the LPS acute lung injury model in mice, demonstrating decreased protein leak into BALF and suppression of lung inflammatory cytokine expression and induction of αSMA. Together these data extend prior work on potentially protective effects of AHR stimulation by FICZ in modulating lung inflammation (41–43). Although these observations align nicely with observations from other

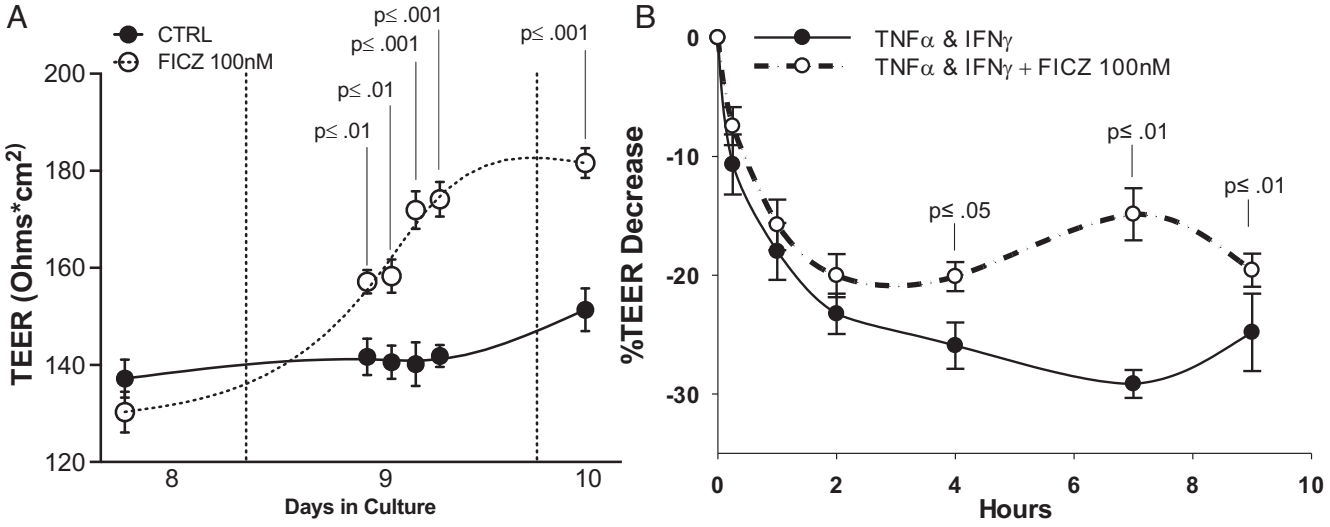

FIGURE 7. AHR activation in primary murine AECs alters membrane permeability. Primary murine AECs were plated on permeable supports immediately after isolation and cultured in media containing FICZ (100 nM) or vehicle control (0.1% DMSO v/v), reaching confluence. (**A**) AECs treated with FICZ sustained higher TEER measurements between days 8 and 10 of culture compared with control-treated AECs. (**B**) AECs were exposed to a combination of TNF-α (100 ng/ml) and IFN-γ (100 ng/ml) for 9 h with or without FICZ (100 nM). The presence of FICZ significantly inhibited the percentage decrease in TEER throughout the course of the study. Data shown are representative of two independent experiments; $n = 6$; paired t test evaluation between treatment groups (filled versus unfilled circles) as indicated at distinct time points.

mucosal organs (44–48), this work brings a focus on AECs and their contributions to the complex innate immune environment in the lung.

A number of recent studies in the lung have focused on the role of AHR in the airways and in the response to cigarette smoke. In the absence of AHR activity, lung neutrophil accumulation and cytokine expression are increased in mice following cigarette smoke exposure (20). Emphysema is also worsened in association with increased evidence of apoptosis, diminished antioxidant expression, and imbalance of proteases-antiproteases (49). AHR activation also suppresses Muc5AC expression and mucus overproduction in a murine model of allergic asthma (50). This effect on mucus production appears to involve suppression of inflammasome activation and mitochondrial ROS (50). Other investigators working in a murine model have identified a potentially significant role of AHR activation early in life for T cell or dendritic cell contributions to adaptive immune responses to influenza (51, 52). In the setting of acute lung injury due to hyperoxia, AHR activation and expression of downstream genes such as *CYP1A1* and *NQO1* may reduce oxidative stress and limit injury (53–55). However, this interaction is quite complex, with differential effects depending on the duration of AHR activation (55, 56). In studies using the bleomycin model of pulmonary fibrosis, Takei and colleagues (21) found that FICZ treatment was associated with reduced fibrosis; increased numbers of T regulatory cells; and decreases in the numbers of T cells expressing IFN-γ, IL-17A, and IL-22. In a related study, Wu and colleagues described a complex balance between the profibrotic effects of IGF-1 and protective effects of AHR activation following exposure to bleomycin (57). Overall, these studies have suggested a role of endogenous AHR activation in the lung in modulating local response to a variety of stresses.

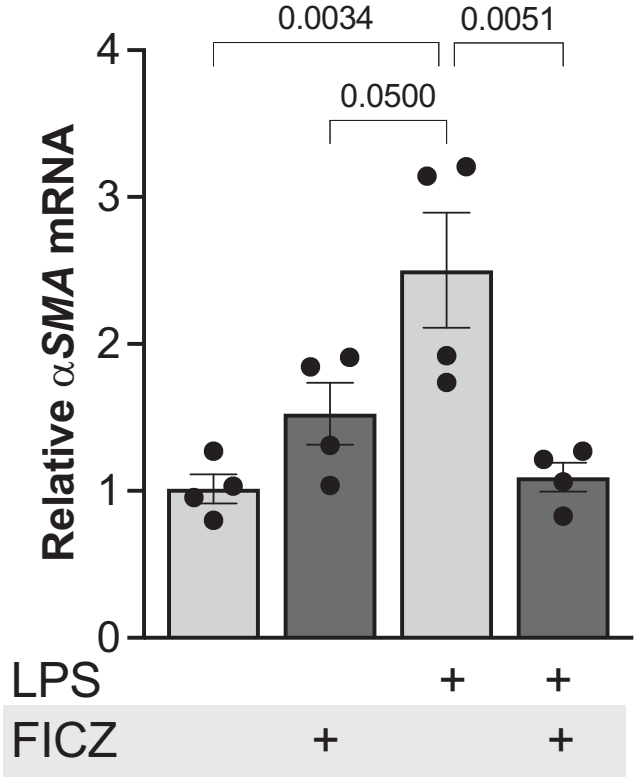

FIGURE 8. Expression of α mRNA in lung homogenates following intranasal inoculation of FICZ and LPS treatments. Experimental replicates as shown; multiple comparison analysis was conducted using ANOVA followed by Tukey post hoc test.

The lung is a complex organ with over 40 different cell types. The effects of AHR activation are often a consequence of activity in a number of different cell types, including both parenchymal and inflammatory cells. Initially appreciated largely for the role in barrier function and as the source of pulmonary surfactant, AECs are important contributors to pulmonary innate immunity. They are critically important for alveolar macrophage maturation and serve as sentinel cells, expressing early response cytokines and chemokines to recruit leukocytes to the alveolar space in response to inflammatory stimulation. It is for this reason that we have focused on TNF-α, IL-1β, and CXCL2 in these studies. The present work extends our understanding of the biology of AECs and of the impact of endogenous activation of AHR in the lung.

There are many potentially overlapping mechanisms by which AHR activation may contribute to alveolar epithelial integrity and

decreased susceptibility to lung injury. AHR activation leads to transcription of a large number of genes influencing apoptosis, autophagy, differentiation, redox balance, and more. AHR also interacts with and modulates activity of transcriptional programs involving Wnt/β-catenin, TGF-β, Notch, and NF-κB (58, 59). The direct effects on early response cytokine expression by AECs and the impact of AHR on epithelial cell expression of mesenchymal genes in vitro suggest dual effects on NF-κB and SMAD signaling. In the context of the LPS model of acute lung injury, it is likely that FICZ-induced AHR activation in other cell types, especially alveolar macrophages, also contributes to limitation of inflammatory cytokine expression through effects on NF-κB activation. Finally, it has become clear that AHR may have noncanonical cytoplasmic activities that do not involve nuclear translocation and transcription factor activity. In particular, cytoplasmic AHR has been found to modulate protein translation (via GSK3β) and degradation (through a ubiquitin E3 ligase activity) to influence the expression of mesenchymal proteins such as vimentin (60). In in vitro studies, these nongenomic effects may be independent of interactions with AHR ligands (61, 62). Although cytoplasmic AHR effects may contribute to limitation of EMT in our studies, the effects of FICZ on EMT gene expression and cytokine gene expression support an important role of transcriptional AHR in these processes.

The time course of AHR activation often depends on the specific ligand involved and can have important implications for the outcome of receptor binding. One important activity of cytochrome P450 enzyme induction following AHR activation is to degrade endogenous AHR ligands (63, 64). Similarly, the AHR repressor is a downstream gene that is induced by AHR activation and that inactivates AHR. These negative feedback mechanisms serve to limit the period of AHR activation in response to endogenous ligands. In contrast, the environmental toxicant TCDD may induce prolonged and dysregulated AHR activation, contributing to its pathological effects (65). In the context of acute epithelial injury, one might hypothesize that early limitation of AHR activity, leading to EMT, could be advantageous for wound closure, followed by AHR activation leading to restoration of normal epithelial cell characteristics and limitation of scar. Our observations that FICZ slowed wound closure in the scratch model, while enhancing TEER in primary AECs, are consistent with this hypothesis.

A strength of this work is the use of primary murine AECs as a model for understanding epithelial cell biology in the alveolar space. However, they are not suitable for CRISPR technology and do not form tight monolayers in vitro. Thus, we have relied on the SV40-transformed MLE-15 murine cell line for our CRISPR experiments knocking down AHR and for the scratch wound studies. We believe the consistency of the picture of AHR's role in studies using different techniques in different models provides important support for our conclusions. Because AHR is widely expressed in the lung, the beneficial effects of FICZ treatment in the LPS model of acute lung injury may reflect contributions of AHR activation in multiple cell types. However, the combination of in vivo and in vitro results strongly supports an important contribution of effects in AECs.

In conclusion, these studies expand the understanding of the role of AHR in AECs. They suggest that AHR activity limits susceptibility to inflammatory lung injury through modulation of the epithelial cell inflammatory response and effects on epithelial barrier function. The former effect is observed in AECs themselves, in addition to potential effects on lung macrophages. Our studies also raise the possibility that activation of AHR following lung injury may suppress dysregulated repair that contributes to fibrosis. Further studies involving the temporal sequence of AHR activation will be necessary to fully understand the potential for therapeutic targeting of AHR and the implications of disruption of this pathway by environmental toxicants.

Acknowledgments

We acknowledge the technical assistance received from Laura Hoffman.

Disclosures

The authors have no financial conflicts of interest.

References

1. Esser, C., and A. Rannug. 2015. The aryl hydrocarbon receptor in barrier organ physiology, immunology, and toxicology. *Pharmacol. Rev.* 67: 259–279.
2. Healey, A. M., K. N. Fenner, C. T. O'Dell, and B. P. Lawrence. 2024. Aryl hydrocarbon receptor activation alters immune cell populations in the lung and bone marrow during coronavirus infection. *Am. J. Physiol. Lung Cell. Mol. Physiol.* 326: L313–L329.
3. Michaudel, C., F. Bataille, I. Maillet, L. Fauconnier, C. Colas, H. Sokol, M. Straube, A. Couturier-Maillard, L. Dumoutier, J. van Snick, et al. 2020. Ozone-induced aryl hydrocarbon receptor activation controls lung inflammation via interleukin-22 modulation. *Front. Immunol.* 11: 144.
4. Vazquez-Gomez, G., M. Karasova, Z. Tylichova, M. Kabatkova, A. Hampl, J. Matthews, J. Neca, M. Ciganek, M. Machala, and J. Vondracek. 2022. Aryl hydrocarbon receptor (AhR) limits the inflammatory responses in human lung adenocarcinoma A549 cells via interference with NF-kappaB signaling. *Cells* 11: 707.
5. Thompson, B. T., R. C. Chambers, and K. D. Liu. 2017. Acute respiratory distress syndrome. *N. Engl. J. Med.* 377: 562–572.
6. Whitsett, J. A., and T. Alenghat. 2015. Respiratory epithelial cells orchestrate pulmonary innate immunity. *Nat. Immunol.* 16: 27–35.
7. Trapnell, B. C., and J. A. Whitsett. 2002. GM-CSF regulates pulmonary surfactant homeostasis and alveolar macrophage-mediated innate host defense. *Annu. Rev. Physiol.* 64: 775–802.
8. Sturrock, A., D. Woller, A. Freeman, K. Sanders, and R. Paine III. 2018. Consequences of hypoxia for the pulmonary alveolar epithelial cell innate immune response. *J. Immunol.* 201: 3411–3420.
9. Crosby, L. M., C. Luellen, Z. Zhang, L. L. Tague, S. E. Sinclair, and C. M. Waters. 2011. Balance of life and death in alveolar epithelial type II cells: proliferation, apoptosis, and the effects of cyclic stretch on wound healing. *Am. J. Physiol. Lung Cell. Mol. Physiol.* 301: L536–L546.
10. Noble, P. W., C. E. Barkauskas, and D. Jiang. 2012. Pulmonary fibrosis: patterns and perpetrators. *J. Clin. Invest.* 122: 2756–2762.
11. Beamer, C. A., and D. M. Shepherd. 2013. Role of the aryl hydrocarbon receptor (AhR) in lung inflammation. *Semin. Immunopathol.* 35: 693–704.
12. Mir-Kasimov, M., A. Sturrock, M. McManus, and R. Paine III. 2012. Effect of alveolar epithelial cell plasticity on the regulation of GM-CSF expression. *Am. J. Physiol. Lung Cell. Mol. Physiol.* 302: L504–511.
13. Sturrock, A., M. Mir-Kasimov, J. Baker, J. Rowley, and R. Paine III. 2014. Key role of microRNA in the regulation of granulocyte macrophage colony-stimulating factor expression in murine alveolar epithelial cells during oxidative stress. *J. Biol. Chem.* 289: 4095–4105.
14. Sturrock, A., E. Seedahmed, M. Mir-Kasimov, J. Boltax, M. L. McManus, and R. Paine III. 2012. GM-CSF provides autocrine protection for murine alveolar epithelial cells from oxidant-induced mitochondrial injury. *Am. J. Physiol. Lung Cell. Mol. Physiol.* 302: L343–L351.
15. Sturrock, A., T. Vollbrecht, M. Mir-Kasimov, M. McManus, S. E. Wilcoxen, and R. Paine III. 2010. Mechanisms of suppression of alveolar epithelial cell GM-CSF expression in the setting of hyperoxic stress. *Am. J. Physiol. Lung Cell. Mol. Physiol.* 298: L446–453.
16. Wikenheiser, K. A., D. K. Vorbroker, W. R. Rice, J. C. Clark, C. J. Bachurski, H. K. Oie, and J. A. Whitsett. 1993. Production of immortalized distal respiratory epithelial cell lines from surfactant protein C/simian virus 40 large tumor antigen transgenic mice. *Proc. Natl. Acad. Sci. U. S. A.* 90: 11029–11033.
17. Ibrahim, M., E. M. MacFarlane, G. Matteo, M. P. Hoyeck, K. R. C. Rick, S. Farokhi, C. M. Copley, S. O'Dwyer, and J. E. Bruin. 2020. Functional cytochrome P450 1A enzymes are induced in mouse and human islets following pollutant exposure. *Diabetologia* 63: 162–178.
18. Kreft, M. E., U. D. Jerman, E. Lasic, N. Hevir-Kene, T. L. Rizner, L. Peternel, and K. Kristan. 2015. The characterization of the human cell line Calu-3 under different culture conditions and its use as an optimized in vitro model to investigate bronchial epithelial function. *Eur. J. Pharm. Sci.* 69: 1–9.
19. Bozinovski, S., J. Jones, S. J. Beavitt, A. D. Cook, J. A. Hamilton, and G. P. Anderson. 2004. Innate immune responses to LPS in mouse lung are suppressed and reversed by neutralization of GM-CSF via repression of TLR-4. *Am. J. Physiol. Lung Cell. Mol. Physiol.* 286: L877–L885.
20. Rico de Souza, A., H. Traboulsi, X. Wang, J. H. Fritz, D. H. Eidelman, and C. J. Baglole. 2021. The aryl hydrocarbon receptor attenuates acute cigarette smoke-induced airway neutrophilia independent of the dioxin response element. *Front. Immunol.* 12: 630427.
21. Takei, H., H. Yasuoka, K. Yoshimoto, and T. Takeuchi. 2020. Aryl hydrocarbon receptor signals attenuate lung fibrosis in the bleomycin-induced mouse model for pulmonary fibrosis through increase of regulatory T cells. *Arthritis Res. Ther.* 22: 20.
22. Goedtke, L., H. Sprenger, U. Hofmann, F. F. Schmidt, H. S. Hammer, U. M. Zanger, O. Poetz, A. Seidel, A. Braeuning, and S. Hessel-Pras. 2020. Polycyclic aromatic hydrocarbons activate the aryl hydrocarbon receptor and the constitutive androstane receptor to regulate xenobiotic metabolism in human liver cells. *Int. J. Mol. Sci.* 22: 372.

23. Sjogren, M., L. Ehrenberg, and U. Rannug. 1996. Relevance of different biological assays in assessing initiating and promoting properties of polycyclic aromatic hydrocarbons with respect to carcinogenic potency. *Mutat. Res.* 358: 97–112.
24. Ko, H. K., A. H. Lin, D. W. Perng, T. S. Lee, and Y. R. Kou. 2020. Lung epithelial TRPA1 mediates lipopolysaccharide-induced lung inflammation in bronchial epithelial cells and mice. *Front. Physiol.* 11: 596314.
25. Resiliac, J., M. Rohlfing, J. Santoro, S.-R. A. Hussain, and M. H. Grayson. 2023. Low-dose lipopolysaccharide protects from lethal paramyxovirus infection in a macrophage- and TLR4-dependent process. *J. Immunol.* 210: 348–355.
26. Xavier, A. M., N. Isowa, L. Cai, E. Dziak, M. Opas, D. I. McRitchie, A. S. Slutsky, S. H. Keshavjee, and M. Liu. 1999. Tumor necrosis factor-alpha mediates lipopolysaccharide-induced macrophage inflammatory protein-2 release from alveolar epithelial cells. Autoregulation in host defense. *Am. J. Respir. Cell. Mol. Biol.* 21: 510–520.
27. Hýžd'alová, M., J. Procházková, S. Strapáčová, L. Svržková, O. Vacek, R. Fedr, Z. Andrysík, E. Hrubá, H. Líbalová, J. Kléma, et al. 2021. A prolonged exposure of human lung carcinoma epithelial cells to benzo[a]pyrene induces p21-dependent epithelial-to-mesenchymal transition (EMT)-like phenotype. *Chemosphere* 263: 128126.
28. Nothdurft, S., C. Thumser-Henner, F. Breitenbucher, R. A. Okimoto, M. Dorsch, C. A. Opitz, A. Sadik, C. Esser, M. Holzel, S. Asthana, et al. 2020. Functional screening identifies aryl hydrocarbon receptor as suppressor of lung cancer metastasis. *Oncogenesis* 9: 102.
29. Naoi, H., Y. Suzuki, A. Miyagi, R. Horiguchi, Y. Aono, Y. Inoue, H. Yasui, H. Hozumi, M. Karayama, K. Furuhashi, et al. 2024. CD109 attenuates bleomycin-induced pulmonary fibrosis by inhibiting TGF-β signaling [abstract]. *Am. J. Respir. Crit. Care Med.* 209: A5191.
30. Pittet, J.-F., M. J. D. Griffiths, T. Geiser, N. Kaminski, S. L. Dalton, X. Huang, L. A. S. Brown, P. J. Gotwals, V. E. Koteliansky, M. A. Matthay, and D. Sheppard. 2001. TGF-β is a critical mediator of acute lung injury. *J. Clin. Invest.* 107: 1537–1544.
31. Barriere, G., P. Fici, G. Gallerani, F. Fabbri, and M. Rigaud. 2015. Epithelial mesenchymal transition: a double-edged sword. *Clin. Transl. Med.* 4: 14.
32. Haensel, D., and X. Dai. 2018. Epithelial-to-mesenchymal transition in cutaneous wound healing: where we are and where we are heading. *Dev. Dyn.* 247: 473–480.
33. Stone, R. C., I. Pastar, N. Ojeh, V. Chen, S. Liu, K. I. Garzon, and M. Tomic-Canic. 2016. Epithelial-mesenchymal transition in tissue repair and fibrosis. *Cell Tissue Res.* 365: 495–506.
34. Chen, M. C., W. W. Chang, Y. D. Kuan, S. T. Lin, H. C. Hsu, and C. H. Lee. 2012. Resveratrol inhibits LPS-induced epithelial-mesenchymal transition in mouse melanoma model. *Innate Immun.* 18: 685–693.
35. Cho, I. H., E. H. Jang, D. Hong, B. Jung, M. J. Park, and J. H. Kim. 2015. Suppression of LPS-induced epithelial-mesenchymal transition by aqueous extracts of *Prunella vulgaris* through inhibition of the NF-kappaB/Snail signaling pathway and regulation of EMT-related protein expression. *Oncol. Rep.* 34: 2445–2450.
36. Vogel, C. F. A., L. S. Van Winkle, C. Esser, and T. Haarmann-Stemmann. 2020. The aryl hydrocarbon receptor as a target of environmental stressors - implications for pollution mediated stress and inflammatory responses. *Redox Biol.* 34: 101530.
37. Anderson, G., A. Carbone, and G. Mazzoccoli. 2021. Tryptophan metabolites and aryl hydrocarbon receptor in severe acute respiratory syndrome, coronavirus-2 (SARS-CoV-2) pathophysiology. *Int. J. Mol. Sci.* 22: 1597.
38. Gargaro, M., G. Manni, G. Scalisi, P. Puccetti, and F. Fallarino. 2021. Tryptophan metabolites at the crossroad of immune-cell interaction via the aryl hydrocarbon receptor: implications for tumor immunotherapy. *Int. J. Mol. Sci.* 22: 4644.
39. Grifka-Walk, H. M., B. R. Jenkins, and D. J. Kominsky. 2021. Amino acid trip: the far out impacts of host and commensal tryptophan metabolism. *Front. Immunol.* 12: 653208.
40. Dolivo, D. M., S. A. Larson, and T. Dominko. 2018. Tryptophan metabolites kynurenine and serotonin regulate fibroblast activation and fibrosis. *Cell. Mol. Life. Sci.* 75: 3663–3681.
41. de Araujo, E. F., F. V. Loures, N. W. Preite, C. Feriotti, N. A. Galdino, T. A. Costa, and V. L. G. Calich. 2021. AhR ligands modulate the differentiation of innate lymphoid cells and T helper cell subsets that control the severity of a pulmonary fungal infection. *Front. Immunol.* 12: 630938.
42. Lee, S.-M., C. E. Kim, H. Y. Park, E. H. Yoon, H. J. Won, J. M. Ahn, N. Z. N. Nguyen, M. Kim, W. H. Jang, W.-S. Lee, et al. 2022. Aryl hydrocarbon receptor–targeted therapy for $CD4^+$ T cell–mediated idiopathic pneumonia syndrome in mice. *Blood* 139: 3325–3339.
43. Liu, K. Y., L. T. Wang, H. C. Wang, S. N. Wang, L. W. Tseng, C. Y. Chai, S. S. Chiou, S. K. Huang, and S. H. Hsu. 2021. Aryl hydrocarbon receptor is essential in the control of lung club cell homeostasis. *J. Inflamm. Res.* 14: 299–311.
44. Dong, F., and G. H. Perdew. 2020. The aryl hydrocarbon receptor as a mediator of host-microbiota interplay. *Gut Microbes* 12: 1859812.
45. Fernandez-Salguero, P., T. Pineau, D. M. Hilbert, T. McPhail, S. S. Lee, S. Kimura, D. W. Nebert, S. Rudikoff, J. M. Ward, and F. J. Gonzalez. 1995. Immune system impairment and hepatic fibrosis in mice lacking the dioxin-binding Ah receptor. *Science* 268: 722–726.
46. Furue, M., A. Hashimoto-Hachiya, and G. Tsuji. 2019. Aryl hydrocarbon receptor in atopic dermatitis and psoriasis. *Int. J. Mol. Sci.* 20: 5424.
47. Liu, Y., Y. Chen, R. Zhu, L. Xu, H. Q. Xie, and B. Zhao. 2021. Rutaecarpine inhibits U87 glioblastoma cell migration by activating the aryl hydrocarbon receptor signaling pathway. *Front. Mol. Neurosci.* 14: 765712.
48. McDonnell, W. M., S. W. Chensue, F. K. Askari, and R. H. Moseley. 1996. Hepatic fibrosis in $ahr^{-/-}$ mice. *Science* 271: 223b–224b.
49. Guerrina, N., H. Traboulsi, A. Rico de Souza, Y. Bosse, T. H. Thatcher, A. Robichaud, J. Ding, P. Z. Li, L. Simon, S. Pareek, et al. 2021. Aryl hydrocarbon receptor deficiency causes the development of chronic obstructive pulmonary disease through the integration of multiple pathogenic mechanisms. *FASEB J.* 35: e21376.
50. Hu, X., Y. Shen, Y. Zhao, J. Wang, X. Zhang, W. Tu, W. Kaufman, J. Feng, and P. Gao. 2021. Epithelial aryl hydrocarbon receptor protects from mucus production by inhibiting ROS-triggered NLRP3 inflammasome in asthma. *Front. Immunol.* 12: 767508.
51. Houser, C. L., and B. P. Lawrence. 2022. The aryl hydrocarbon receptor modulates T follicular helper cell responses to influenza virus infection in mice. *J. Immunol.* 208: 2319–2330.
52. Lawrence, B. P., A. D. Roberts, J. J. Neumiller, J. A. Cundiff, and D. L. Woodland. 2006. Aryl hydrocarbon receptor activation impairs the priming but not the recall of influenza virus-specific $CD8^+$ T cells in the lung. *J. Immunol.* 177: 5819–5828.
53. Lingappan, K., W. Jiang, L. Wang, G. Wang, X. I. Couroucli, B. Shivanna, S. E. Welty, R. Barrios, M. F. Khan, D. W. Nebert, et al. 2014. Mice deficient in the gene for cytochrome P450 (CYP)1A1 are more susceptible than wild-type to hyperoxic lung injury: evidence for protective role of CYP1A1 against oxidative stress. *Toxicol. Sci.* 141: 68–77.
54. Shivanna, B., C. Chu, and B. Moorthy. 2022. The aryl hydrocarbon receptor (AHR): a novel therapeutic target for pulmonary diseases? *Int J Mol Sci* 23: 1516.
55. Shivanna, B., C. Chu, S. E. Welty, W. Jiang, L. Wang, X. I. Couroucli, and B. Moorthy. 2011. Omeprazole attenuates hyperoxic injury in H441 cells via the aryl hydrocarbon receptor. *Free Radic. Biol. Med.* 51: 1910–1917.
56. Shivanna, B., S. Zhang, A. Patel, W. Jiang, L. Wang, S. E. Welty, and B. Moorthy. 2015. Omeprazole attenuates pulmonary aryl hydrocarbon receptor activation and potentiates hyperoxia-induced developmental lung injury in newborn mice. *Toxicol. Sci.* 148: 276–287.
57. Wu, S. M., J. J. Tsai, H. C. Pan, J. L. Arbiser, L. Elia, and M. L. Sheu. 2022. Aggravation of pulmonary fibrosis after knocking down the aryl hydrocarbon receptor in the insulin-like growth factor 1 receptor pathway. *Br. J. Pharmacol.* 179: 3430–3451.
58. Larigot, L., L. Juricek, J. Dairou, and X. Coumoul. 2018. AhR signaling pathways and regulatory functions. *Biochim. Open* 7: 1–9.
59. Liu, Z., L. Li, W. Chen, Q. Wang, W. Xiao, Y. Ma, B. Sheng, X. Li, L. Sun, M. Yu, and H. Yang. 2018. Aryl hydrocarbon receptor activation maintained the intestinal epithelial barrier function through Notch1 dependent signaling pathway. *Int. J. Mol. Med.* 41: 1560–1572.
60. Li, C. H., C. W. Liu, C. H. Tsai, Y. J. Peng, Y. H. Yang, P. L. Liao, C. C. Lee, Y. W. Cheng, and J. J. Kang. 2017. Cytoplasmic aryl hydrocarbon receptor regulates glycogen synthase kinase 3 beta, accelerates vimentin degradation, and suppresses epithelial-mesenchymal transition in non-small cell lung cancer cells. *Arch. Toxicol.* 91: 2165–2178.
61. Opitz, C. A., P. Holfelder, M. T. Prentzell, and S. Trump. 2023. The complex biology of aryl hydrocarbon receptor activation in cancer and beyond. *Biochem. Pharmacol.* 216: 115798.
62. Sondermann, N. C., S. Faßbender, F. Hartung, A. M. Hätälä, K. M. Rolfes, C. F. A. Vogel, and T. Haarmann-Stemmann. 2023. Functions of the aryl hydrocarbon receptor (AHR) beyond the canonical AHR/ARNT signaling pathway. *Biochem. Pharmacol.* 208: 115371.
63. Delescluse, C., G. Lemaire, G. de Sousa, and R. Rahmani. 2000. Is CYP1A1 induction always related to AHR signaling pathway? *Toxicology* 153: 73–82.
64. Ma, Q. 2001. Induction of CYP1A1. The AhR/DRE paradigm: transcription, receptor regulation, and expanding biological roles. *Curr. Drug. Metab.* 2: 149–164.
65. Sorg, O. 2014. AhR signalling and dioxin toxicity. *Toxicol. Lett.* 230: 225–233.